Thin Solid Films 570 (2014) 298–302

Contents lists available at ScienceDirect

Thin Solid Films

journal homepage: www.elsevier.com/locate/tsf

Light-activated gas sensing of Bi_2O_3-core/ZnO-shell nanobelt gas sensors

Sunghoon Park [a], Hyunsung Ko [a], Sangmin Lee [b], Hyounwoo Kim [c], Chongmu Lee [a,*]

[a] Department of Materials Science and Engineering, Inha University, 253 Yonghyun-Dong, Nam-gu, Incheon 402-751, Republic of Korea
[b] Department of Electronic Engineering, Inha University, 253 Yonghyun-Dong, Nam-gu, Incheon 402-751, Republic of Korea
[c] Division of Materials Science and Engineering, Hanyang University, Seoul 133-791, Republic of Korea

ARTICLE INFO

Available online 15 March 2014

Keywords:
Bi_2O_3
ZnO
Nanobelts
Sensor
Response

ABSTRACT

Bi_2O_3 is highly sensitive to low concentrations of NO_2 in ambient air but almost insensitive to most other common gasses. On the other hand, its sensing performance and detection limit need to be improved before it can be used more widely. This study examined the NO_2 gas sensing properties of β-Bi_2O_3 nanobelts encapsulated with ZnO. Bi_2O_3-core/ZnO-shell nanobelts were fabricated using a two-step process involving the thermal evaporation of Bi powders and the atomic layer deposition of ZnO. The core–shell nanobelts were 100 to 300 nm in diameter with lengths ranging from a few tens to a few hundreds of micrometers with a mean shell layer thickness of ~20 nm. Multiple networked Bi_2O_3-core/ZnO-shell nanobelt sensors showed responses of 113–198% and 227–665% to 1–5 ppm NO_2 at room temperature in the dark and under UV illumination, respectively. These responses were 1.2–1.9 and 2.4–6.3 times larger, respectively, than those of pristine Bi_2O_3 nanobelt sensors at 1–5 ppm NO_2. The underlying mechanism of the enhanced response of the Bi_2O_3 nanobelts to NO_2 gas by ZnO encapsulation and UV irradiation is discussed.

1. Introduction

Bismuth oxide (Bi_2O_3) is an important wide band gap semiconductor with four main crystallographic polymorphs denoted as α-, β-, γ-, and δ-Bi_2O_3 [1]. Of these polymorphs, α- and δ-Bi_2O_3 are p-type semiconductors, whereas β-Bi_2O_3 is an n-type semiconductor. Owing to its unique physical properties, such as a large energy band gap, high refractive index, dielectric permittivity and high oxygen conductivity, as well as its remarkable photoconductivity and photoluminescence [2–4], Bi_2O_3 has been studied extensively for a range of applications, such as gas sensors, photovoltaic cells, optical coatings, fuel cells, supercapacitors and photocatalysts [1,5–7]. Regarding gas sensor applications, one-dimensional (1D) nanostructures are expected to show a considerably enhanced performance because of their ultrahigh surface-to-volume ratios and Debye length comparable to their dimensions [8], which makes their electrical properties extremely sensitive to surface-adsorbed species. Bismuth oxide 1D nanostructures have been prepared using a range of techniques such as metal–organic chemical vapor deposition [9], chemical methods [10], oxidative metal vapor transport deposition techniques [11], solution chemical methods [12], and stress-induced methods [13]. On the other hand, the use of the vapor–liquid–solid (VLS) method to synthesize Bi_2O_3 1D nanostructures, has not been reported, despite it being most successful in generating 1D nanostructures with single crystalline structures and in relatively large quantities [14].

Bi_2O_3 1D nanostructures are quite sensitive to low concentrations of NO_2 in ambient air but are almost insensitive to most other common gasses [12]. Nevertheless, enhancing their sensing performance and detection limits remains a challenge. Several techniques, such as surface functionalization [15–17], doping [18–20], core–shell structure formation [21–23] and UV irradiation [24–26], have been developed to enhance the sensing performance, detection limit and operation temperature of 1D nanostructure sensors. On the other hand, the effects of a combination of two of these techniques on the sensing properties of Bi_2O_3 1D nanostructure sensors have not been reported. In this study, multiple networked Bi_2O_3-core/ZnO-shell nanobelt sensors were fabricated and their NO_2 gas sensing properties under UV illumination were examined to determine the combinational effects of core–shell structure formation and UV irradiation on the gas sensing properties of Bi_2O_3 1D nanostructures.

2. Experimental details

Bi_2O_3-core/ZnO-shell nanobelts were synthesized using a two-step process: the thermal evaporation of bismuth (Bi) powders in an oxidizing atmosphere and the atomic layer deposition of ZnO. First, Au-coated sapphire was used as a substrate for the synthesis of Bi_2O_3 nanostructures. Au was deposited on a c-plane sapphire substrate by direct current (dc) magnetron sputtering. A quartz tube was mounted horizontally inside a tube furnace. Bi powders (99.99% purity) were placed on the lower holder at the center of the quartz tube. An Au-coated sapphire substrate was placed on the upper holder, approximately 5 mm away from the source powders. The furnace was heated to 650 °C and

* Corresponding author. Tel.: +82 32 860 7536; fax: +82 32 862 5546.
E-mail address: cmlee@inha.ac.kr (C. Lee).

http://dx.doi.org/10.1016/j.tsf.2014.02.110
0040-6090/

maintained at that temperature for 1 h in a N_2/1 vol.%-O_2 atmosphere with constant flow rates of oxygen (O_2) (3 cm^3/min) and N_2 (500 cm^3/min). The total pressure was set to 133 Pa. The as-synthesized Bi_2O_3 nanobelts were then transferred to an atomic layer deposition (ALD) chamber and coated with ZnO. For this diethylzinc (DEZn) and H_2O were kept in bubblers at 10 °C. These source gasses were fed alternatively into the chamber through separate inlet lines and nozzles. The typical pulse lengths were 0.15 s for DEZn (0 °C), 0.2 s for H_2O (10 °C) and 3 s for purging the reactants. The substrate temperature, pressure and number of ALD process cycles in the chamber were 150 °C, 13.3 Pa and 50, respectively.

The morphology of the products was examined by field emission scanning electron microscopy (FESEM, Hitachi S-4200, V = 15 kV). The microstructures and compositions of the nanobelt samples were characterized further by transmission electron microscopy (TEM, Phillips CM-200, V = 200 kV). Glancing angle X-ray diffraction (XRD, Philips X'pert MRD) was performed at a scan rate of 2/min using Cu-K_α radiation to identify the morphology and structure of the nanobelt samples. The samples were arranged geometrically at a 0.5° glancing angle with a rotating detector.

For the sensing measurements, a 300 nm thick SiO_2 film was grown thermally on the single crystalline Si (100). Ni (~10 nm in thickness) and Au (~50 nm) thin films were deposited sequentially by sputtering to form electrodes on the SiO_2-coated Si substrates using an interdigital electrode (IDE) mask. Multiple networked Bi_2O_3-core/ZnO-shell nanobelt gas sensors were fabricated by pouring a few drops of nanobelt-suspended ethanol onto the oxidized Si substrates equipped with a pair of IDEs with a gap length of 20 μm. The NO_2 (>99.99%) test gas was mixed with synthetic air to achieve the desired concentration, and the flow rate was maintained at 200 cm^3/min using a mass flow controller to obtain NO_2 concentrations of 1–5 ppm. A Keithley sourcemeter-2612 was used to measure the resistance. The sourcemeter was connected to a computer via a universal serial bus connector. The electrical resistance of the gas sensors was determined in the dark and under UV light (λ = 254 nm) illumination at 1.2 mW/cm^2 at 25 °C by measuring the electric current at room temperature that flowed when a potential difference of 0.5 V had been applied between the Ni/Au IDEs. The response was defined as $(R_g - R_a)$ / R_a for NO_2 gas, where R_a and R_g are the electrical resistances of the sensors in air and target gas, respectively. The response time was defined as the time required for the change in electrical resistance to reach 90% of the equilibrium value after injecting NO_2, and the recovery time was defined as the time needed for the sensor to return to 90% above the original resistance in air after removing the NO_2 gas.

3. Result and discussion

Fig. 1 shows a FESEM image of the Bi_2O_3-core/ZnO-shell 1D nanostructures synthesized in this study. The nanobelts ranged from 100 to 300 nm in diameter with lengths ranging from a few tens to a few hundreds of micrometers (Fig. 1). An enlarged FESEM image of a typical 1D nanostructure revealed a belt-like or sheet-like morphology (inset in Fig. 1). Fig. 2 shows XRD patterns of the as-synthesized Bi_2O_3-core/ZnO-shell nanobelts. All the reflection peaks in the pattern of the as-synthesized core–shell nanobelts could be assigned to a monoclinic structure, which is in good agreement with the data reported for bulk β-Bi_2O_3 crystals (JCPDS card no. 76-1730, a = 0.5830 nm, b = 0.8140 nm, c =0.7480 nm, β = 67.07°), indicating that the nanomaterial is β-Bi_2O_3. No noticeable XRD peaks assigned to wurtzite or zinc blend structured-ZnO were present, indicating that the amount of ZnO is much smaller than that of Bi_2O_3 in the core–shell nanobelt structures. Fig. 3 shows the TEM image of a typical Bi_2O_3-core/ZnO-shell nanobelt. The thickness of the ZnO shell layer was fairly uniform along the axis of the nanobelt, as expected from its formation method, ALD. The mean shell layer thickness was ~20 nm.

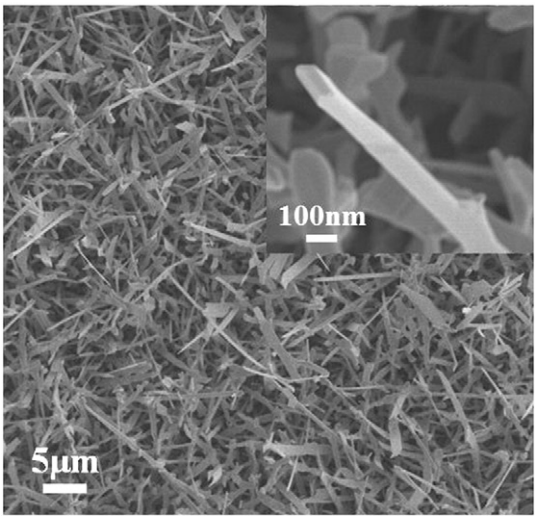

Fig. 1. (a) SEM image of the Bi_2O_3-core/ZnO-shell nanobelts. Inset, enlarged SEM image of a typical Bi_2O_3-core/ZnO-shell nanobelt.

Fig. 4a shows the dynamic responses of the pristine Bi_2O_3 nanobelts in the dark, Bi_2O_3-core/ZnO-shell nanobelts in the dark and Bi_2O_3-core/ZnO-shell nanobelts under UV illumination at room temperature to a typical oxidizing gas NO_2. The resistance increased upon exposure to NO_2 and then decreased upon the removal of NO_2, but it did not recover completely to the initial value upon removal of NO_2. Fig. 4b, c and d, respectively, shows an enlarged part of the data in Fig. 4a measured at a NO_2 concentration of 5 ppm for Bi_2O_3-core/ZnO-shell nanobelts under UV illumination (blue line), Bi_2O_3-core/ZnO-shell nanobelts in the dark (red line), and pristine Bi_2O_3 nanobelts in the dark (black line) to reveal the moments of the gas input and gas stop. The pristine Bi_2O_3 nanobelts showed responses in a range of approximately 95–106% at NO_2 concentrations of 1–5 ppm (Table 1). In contrast, the Bi_2O_3-core/ZnO-shell nanobelts showed responses of approximately 113–198% and 227–665% at 1–5 ppm NO_2 at room temperature in the dark and under UV illumination, respectively. Therefore, the responses of the core–shell nanobelt sensors in the dark and under UV illumination are 1.2–1.9 and 2.4–6.3 times higher, respectively, than those of the pristine Bi_2O_3 nanobelt sensors at 1–5 ppm NO_2.

Table 1 lists the responses of the ZnO-based nanomaterials Bi_2O_3-core/ZnO-shell nanobelts to NO_2 gas in the dark and under UV illumination with those of ZnO-base nanomaterials reported previously [27–29]. A

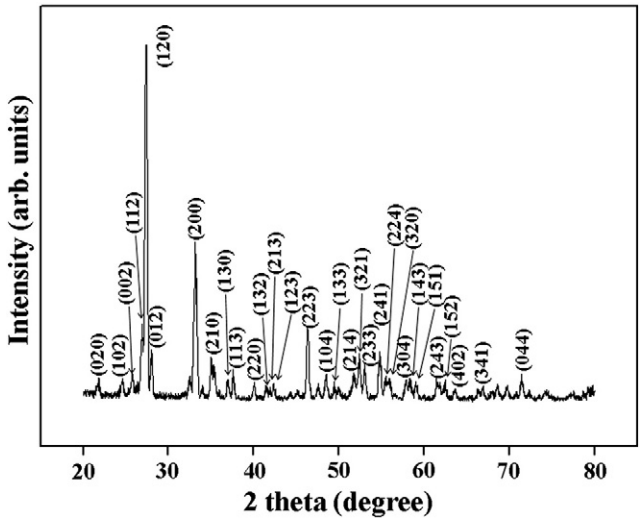

Fig. 2. XRD pattern of the Bi_2O_3-core/ZnO-shell nanobelts.

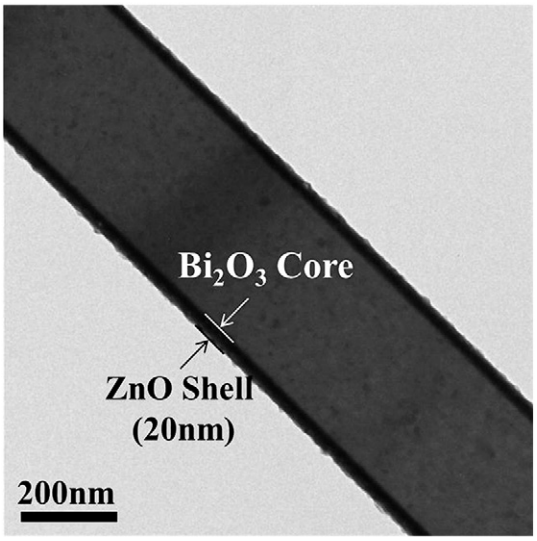

Fig. 3. TEM image of a typical Bi_2O_3-core/ZnO-shell nanobelt.

direct comparison was impossible because of the different sensing test conditions. The reported sensitivity data in Table 1 reported previously was obtained at 250 and 350 °C. In particular, in the case of the ZnO nanowires showing the highest sensitivity the sensing test was carried out, at a higher NO_2 concentration (20 ppm) than in the present study (5 ppm). Generally, the sensitivity of a gas sensor depends strongly on the test temperature. In the present case the response of the Bi_2O_3-core/ZnO-shell nanobelts to NO_2 under UV illumination was stronger than that of the ZnO-based 1D nanostructures even though the test temperature and NO_2 concentration were lower.

Table 1
Sensitivities (or responses) of the 1D ZnO nanostructures to NO_2 gas.

Nanostructures	Temp. (°C)	NO_2 conc.	Sensitivity	Reference
Bi_2O_3/ZnO nanobelts (dark)	25	5 ppm	198%	[Present work]
Bi_2O_3/ZnO nanobelts (UV)	25	5 ppm	665%	[Present work]
ZnO nanowires (dark)	250	20 ppm	9,500%	[28]
ZnO nanorods (dark)	250	0.1 ppm	824%	[29]
ZnO nanobelts (dark)	350	8.5 ppm	81%	[30]

The enhanced response of the Bi_2O_3-core/ZnO-shell nanobelts to NO_2 gas compared with that of the pristine Bi_2O_3 nanobelts can be explained by an expansion of the depletion layer in the Bi_2O_3 core due to electron trapping by the surface states at the Bi_2O_3–ZnO interface [30,31]. The Bi_2O_3–ZnO interface contain a high density of surface states. Electrons near the interface are trapped by the acceptor-type surface states at the interface, resulting in depletion regions in both the Bi_2O_3 core and ZnO shell. Actually, the ZnO shell layer thickness (~20 nm) is smaller than the width of the surface depletion layer in ZnO, which is the order of the Debye length of ZnO (~30 nm) [32]. Consequently, the depletion region in the vicinity of the Bi_2O_3–ZnO interface overlaps the surface depletion region of the ZnO shell. In other words, the entire ZnO shell and a part of the Bi_2O_3 core near the Bi_2O_3–ZnO interface

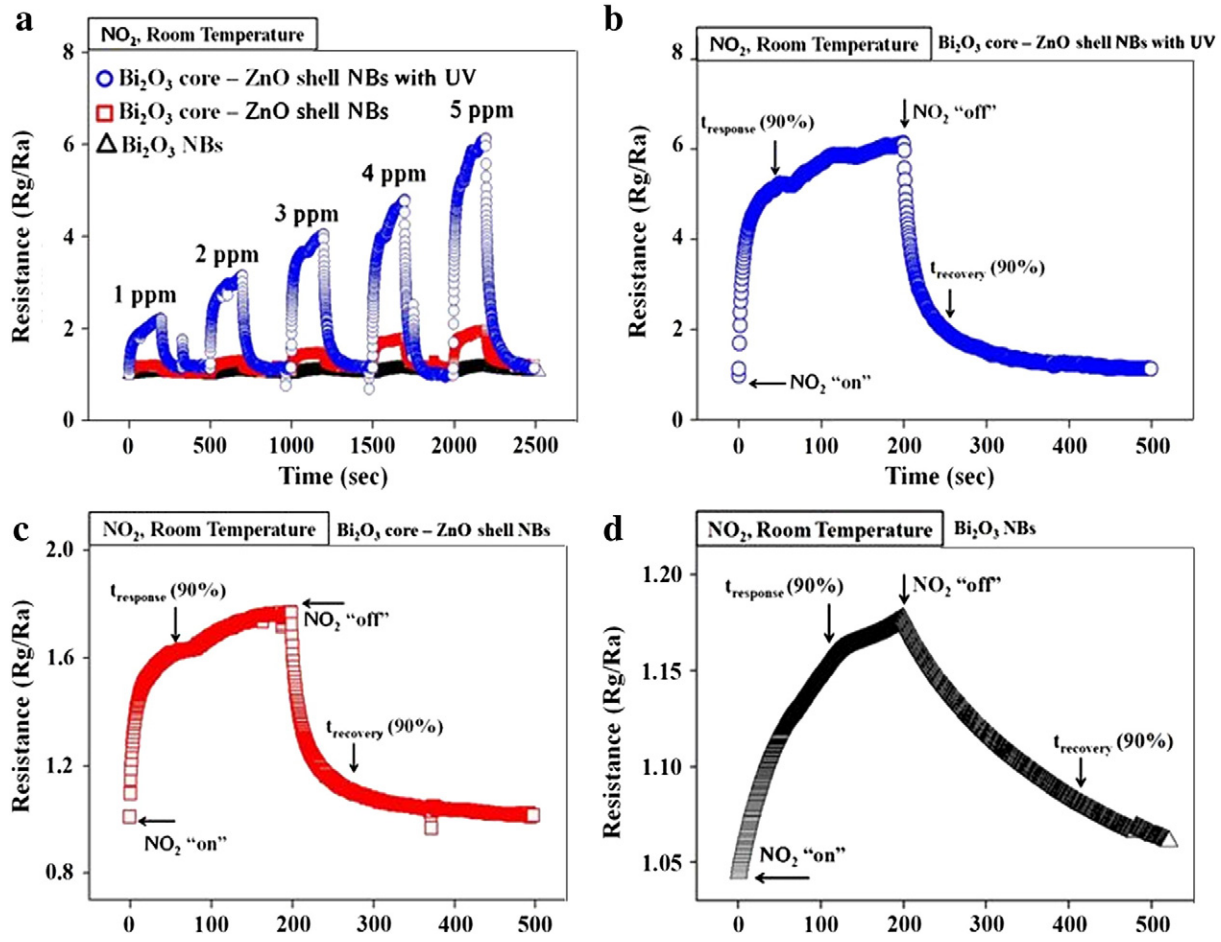

Fig. 4. (a) Dynamic responses of the pristine Bi_2O_3 nanobelts in the dark, Bi_2O_3-core/ZnO-shell nanobelts in the dark and Bi_2O_3-core/ZnO-shell nanobelts under UV illumination at 25 °C. (b) Enlarged part of the Bi_2O_3-core/ZnO-shell nanobelt sensor at 5 ppm NO_2 under UV illumination in (a). (c) Enlarged part of the Bi_2O_3-core/ZnO-shell nanobelt sensor at 5 ppm NO_2 in the dark in (a). (d) Enlarged part of the pristine Bi_2O_3 nanobelt sensor at 5 ppm NO_2 in the dark in (a).

are depleted. The depletion layer in the Bi_2O_3 core must be expanded by electron trapping at the Bi_2O_3–ZnO interface. The larger depletion layer width will result in higher gas sensitivity.

On the other hand, the enhanced NO_2 response of the Bi_2O_3-core/ZnO-shell nanobelt sensor under UV illumination can be explained by the larger number of electrons participating in the reactions with NO_2 molecules because of the photo-generated electron–hole pairs and the increased depletion layer width due to the higher density of electron trap [33,34]. When the core–shell nanobelt is exposed to air, it interacts with oxygen by transferring electrons from the conduction band to the adsorbed oxygen atoms, forming ionic species, such as O^-, O^{2-} and O_2^-. A depletion layer is created in the surface region of the core–shell nanobelt due to the consumption of electrons in the surface region of the core–shell nanobelt. Electron–hole pairs will be generated in the ZnO shell upon exposure to UV light with a photon energy larger than the band gap of the ZnO. During migration to the surface of the ZnO shell, some of the photo-generated electrons and holes will recombine with each other and many of the remaining photo-generated holes will react with negatively charged oxygen ions adsorbed on the surface [25]. The surface depletion layer width is reduced in the ZnO shell of each core–shell nanobelt because of these reactions.

Upon exposure to NO_2 gas, NO_2 gas adsorbs onto the ZnO shells. The remaining photo-generated electrons are released from the shells, and are attracted to the adsorbed NO_2 molecules because an oxidizing gas, e.g. NO_2, acts as an electron acceptor, as shown in the following reactions [35]:

$$NO_2(g) + e^-(h\nu) \rightarrow 2NO(h\nu) + O_2{}^-(h\nu). \quad (2)$$

This reaction widens the surface depletion region in the ZnO shell, resulting in an increase in the resistance of the nanobelt sensor. Therefore, the depletion layer width and electrical resistance of the sensor increase with increasing NO_2 concentration and UV illumination intensity due to an increase in the number of electrons participating in the above reactions.

Overall, the substantial enhancement in the response of the core–shell nanobelts to NO_2 gas by UV irradiation might be the result of a larger change in resistance caused by the increased number of electrons participating in the reactions with NO_2 molecules because of the photo-generated electron–hole pairs and increased depletion layer width due to a higher density of electron trapping. These results show that a synergistic effect on the gas sensing properties of nanostructure sensors can be achieved using a combination of two different techniques. This data is expected to contribute to the development of high performance gas sensors that can be operated at room temperature.

4. Conclusions

Bi_2O_3-core/ZnO-shell nanobelts with a very uniform shell layer thickness were fabricated using a two-step process comprising the thermal evaporation of Bi powders and the atomic layer deposition of ZnO. The multiple networked Bi_2O_3-core/ZnO-shell nanobelt sensors showed the responses of 113–198% and 227–665% to 1–5 ppm NO_2 at room temperature in the dark and under UV illumination, respectively. These responses were 1.2–1.9 and 2.4–6.3 times larger, respectively, than those of the pristine Bi_2O_3 nanobelt sensors at 1–5 ppm NO_2.

The enhanced response of Bi_2O_3-core/ZnO-shell nanobelts to NO_2 gas can be explained based on the energy barrier at the Bi_2O_3–ZnO junction. The energy barrier at the junction acts as a lever in electron transfer through which electron transfer is facilitated or restrained, resulting in enhanced sensing properties of the core–shell nanobelt sensor. On the other hand, the enhanced response of the Bi_2O_3-core/ZnO-shell nanobelts to NO_2 gas under UV illumination is due to the larger change in resistance caused by an increase in the number of electrons participating in the reactions with NO_2 molecules as a result of the photo-generated electron–hole pairs. The energy barrier at the heterojunction is larger under UV illumination than in the dark and increases with increasing UV illumination intensity because more electrons are trapped by the heterojunction under UV illumination.

Acknowledgment

This study was supported by Basic Science Research Program through the National Research Foundation of Korea (NRF) funded by the Ministry of Education (2010-0020163).

References

[1] A. Cabot, A. Marsal, J. Arbiol, J.R. Morante, Bi_2O_3 as a selective sensing material for NO detection, Sens. Actuators B 99 (2004) 74.
[2] V. Fruth, M. Popa, D. Berger, R. Ramer, M. Gartner, A. Ciulei, M. Zaharescu, Deposition and characterization of bismuth oxide thin films, J. Eur. Ceram. Soc. 25 (2005) 2171.
[3] H.T. Fan, X.M. Teng, S.S. Pan, C. Ye, G.H. Li, L.D. Zhang, Optical properties of Bi_2O_3 thin films grown by reactive sputtering, Appl. Phys. Lett. 87 (2005) 231916.
[4] R.L. Thayer, C.A. Randall, S. Trolier-McKinstry, Medium permittivity bismuth zinc niobate thin film capacitors, J. Appl. Phys. 94 (2003) 1941.
[5] K. Sardar, T. Fang, T.W. Yang, A novel route involving an in situ chemical reduction process to the one-dimensional nanostructures of bismuth trioxide, J. Am. Ceram. Soc. 90 (2007) 4033.
[6] T.P. Gujar, V.R. Shinde, C.D. Lokhande, S.H. Han, Electrosynthesis of Bi_2O_3 thin films and their use in electrochemical supercapacitors, J. Power Sources 161 (2006) 1479.
[7] L. Zhou, W. Wang, H. Xu, S. Sun, M. Shang, Bi_2O_3 hierarchical nanostructures: controllable synthesis, growth mechanism, and their application in photocatalysis, Chem. Eur. J. 15 (2009) 1776.
[8] G. Shen, P. Chen, K. Ryu, C.J. Zhou, Devices and chemical sensing applications of metal oxide nanowires, J. Mater. Chem. 19 (2009) 828.
[9] H.W. Kim, J.H. Myung, S.H. Shim, One-dimensional structures of Bi_2O_3 synthesized via metalorganic chemical vapor deposition process, Solid State Commun. 137 (2006) 196.
[10] T.P. Gujar, V.R. Shinde, C.D. Lokhande, S.H. Han, Fibrous nanorod network of bismuth oxide by chemical method, Mater. Sci. Eng. B 133 (2006) 177.
[11] Y. Qiu, D. Liu, J. Yang, S. Yang, Controlled synthesis of bismuth oxide nanowires by an oxidative metal vapor transport deposition technique, Adv. Mater. 8 (2006) 2604.
[12] X. Gou, R. Li, G. Wang, Z. Chen, D. Wexler, Room-temperature solution synthesis of Bi_2O_3 nanowires for gas sensing application, Nanotechnol 20 (2009) (495501-495501-5).
[13] Y.W. Park, H.J. Jung, S.G. Yoon, Bi_2O_3 nanowire growth from high-density Bi nanowires grown at a low temperature using aluminum–bismuth co-deposited films, Sens. Actuators B 156 (2011) 709.
[14] Y. Lu, J. Zhong, Todd Steiner (Eds.), Semiconductor Nanostructures for Optoelectronic Applications, Artech House, Inc., Norwood, MA, 2004, p. 191.
[15] G. Gundiah, A. Govindaraj, C.N.R. Rao, Nanowires, nanobelts and related nanostructures of Ga_2O_3, Chem. Phys. Lett. 351 (2002) 189.
[16] H.Z. Zhang, Y.C. Kong, Y.Z. Wang, X. Du, Z.G. Bai, J.J. Wang, D.P. Yu, Y. Ding, Q.L. Hang, S.Q. Feng, Ga_2O_3 nanowires prepared by physical evaporation, Solid State Commun. 109 (1999) 677.
[17] B.C. Kim, K.T. Sun, K.S. Park, K.J. Im, T. Noh, M.Y. Sung, S. Kim, S. Nahm, Y.N. Choi, S.S. Park, β-GaO nanowires synthesized from milled GaN powders, Appl. Phys. Lett. 80 (2002) 479.
[18] H. Kim, S. Park, C. Jin, C. Lee, Enhanced gas sensing properties of p-type TeO_2 nanorods functionalized with Pd, Nano 6 (2011) 455.
[19] Y.H. Gao, Y. Bando, T. Sato, Y.F. Zhang, X.Q. Gao, Synthesis, Raman scattering and defects of β-GaO nanorods, Appl. Phys. Lett. 81 (2002) 2267.
[20] C.C. Tang, S.S. Fan, M.L. de la Chapelle, P. Li, Silica-assisted catalytic growth of oxide and nitride nanowires, Chem. Phys. Lett. 333 (2001) 12.
[21] M.A. Sanchez-Castillo, C. Couto, W.B. Kim, J.A. Dumestic, Gold-nanotube membranes for the oxidation of CO at gas–water interfaces, Angew. Chem. 116 (2004) 1160.
[22] G. Jágerszki, R.E. Gyurcsányi, L. Höfler, E. Pretsch, Hybridization-modulated ion fluxes through peptide-nucleic-acid-functionalized gold nanotubes. A new approach to quantitative label-free DNA analysis, Nano Lett. 7 (2007) 1609.
[23] Y. Oshima, A. Onga, Helical gold nanotube synthesized at 150 K, Phys. Rev. Lett. 91 (2003) (205503-205503(4)).
[24] C.L. Cao, C.G. Hu, X. Wang, S.X. Wang, Y.S. Tian, H.L. Zhang, UV sensor based on TiO_2 nanorod arrays on FTO thin film, Sens. Actuators B. 156 (2011) 114.
[25] S.W. Fan, A.K. Srivastava, V.P. Dravid, UV-activated room-temperature gas sensing mechanism of polycrystalline ZnO, Appl. Phys. Lett. 95 (2009) (142106-142106(3)).
[26] J. Gong, Y.H. Li, X.S. Chai, Z.S. Hu, Y.L. Deng, UV-light-activated ZnO fibers for organic gas sensing at room temperature, J. Phys. Chem. C 114 (2010) 1293.
[27] E. Oh, H.Y. Choi, S.H. Jung, S. Cho, J.C. Kim, K.H. Lee, S.W. Kang, J. Kim, J.Y. Yun, S.H. Jeong, High-performance NO_2 gas sensor based on ZnO nanorod grown by ultrasonic irradiation, Sens. Actuators B. 141 (2009) 239.
[28] A.Z. Sadek, S. Choopun, W. Wlodarski, S.J. Ippolito, K. Kalantar-Zadeh, Characterization of ZnO nanobelt-based gas sensor for H_2, NO_2, and hydrocarbon sensing, IEEE. Sens. J. 7 (2007) 919.
[29] C.L. Zhu, Y.J. Chen, R.X. Wang, L.J. Wang, M.S. Cao, X.L. Shi, Synthesis and enhanced ethanol sensing properties of α-Fe_2O_3/ZnO heteronanostructures, Sens. Actuators B 140 (2009) 185.

[30] R.W.J. Scott, S.M. Yang, G. Chabanis, N. Coombs, D.E. Williams, G.A. Ozin, Tin dioxide opals and inverted opals: near-ideal microstructures for gas sensors, Adv. Mater. 13 (2001) 1468.
[31] H. Ogawa, M. Nishikawa, A. Abe, Hall measurement studies and an electrical conduction model of tin oxide ultrafine particle films, J. Appl. Phys. 53 (1982) 4448.
[32] N. Barsan, U. Weimar, Conduction model of metal oxide gas sensors, J. Electroceram. 7 (2001) 143.
[33] K.L. Hardee, A.J. Bard, X., Photoelectrochemical behavior of several polycrystalline metal oxide electrodes in aqueous solutions, J. Electrochem. Soc. 124 (1977) 215.
[34] E. McCafferty, A surface charge model of corrosion pit initiation and of protection by surface alloying, J. Electrochem. Soc. 146 (1999) 2863.
[35] E. Comini, A. Cristalli, G. Faglia, G. Sberveglieri, Light enhanced gas sensing properties of indium oxide and tin dioxide sensors, Sens. Actuators B. 65 (2000) 260.